



## ORIGINAL ARTICLE

# Corrosion inhibition of Q235 and X65 steels in CO<sub>2</sub>-saturated solution by 2-phenyl imidazoline



Hua Jiang<sup>a</sup>, Bin Wang<sup>a,\*</sup>, Jie Liu<sup>b</sup>, Jie Zhou<sup>a</sup>, Chunmiao Liu<sup>a</sup>

<sup>a</sup> School of Chemistry and Materials Science, Ludong University, Yantai 264025, PR China

<sup>b</sup> College of Chemistry and Chemical Engineering, Yantai University, Yantai 264005, PR China

Received 14 January 2023; accepted 28 February 2023

Available online 6 March 2023

## KEYWORDS

CO<sub>2</sub> corrosion;  
2-phenyl imidazoline;  
Electrochemical tests;  
Microstructure;  
Adsorption mechanism

**Abstract** This study examined 2-phenyl imidazoline (2-PI) as an eco-friendly corrosion inhibitor for Q235 and X65 steels with various microstructures in CO<sub>2</sub>-saturated solution. The inhibition performances of the 2-PI inhibitor for both steels were comparatively studied through electrochemical tests, weight-loss method, wire beam electrode (WBE) technique as well as surface analysis. The results demonstrate that the 2-PI compound acts as a mixed-type inhibitor and exhibits effective and durable inhibition performance against general and localized corrosion. The adsorption of 2-PI molecules on steel surfaces is exothermic, spontaneous and follows the Langmuir isotherm model. Furthermore, the steel microstructure strongly influences the adsorption behavior of 2-PI inhibitor, the Q235 steel with a higher pearlite/ferrite ratio promotes the physical adsorption of the protonated 2-PI molecules at lower concentrations, and the X65 steel with a lower pearlite/ferrite ratio enhances the chemical adsorption of the unprotonated 2-PI molecules at higher concentrations. Additionally, the adsorption mechanism was also discussed based on the evaluated thermodynamic data and the results of X-ray photoelectron spectroscopy (XPS) analysis.

© 2023 The Author(s). Published by Elsevier B.V. on behalf of King Saud University. This is an open access article under the CC BY-NC-ND license (<http://creativecommons.org/licenses/by-nc-nd/4.0/>).

## 1. Introduction

The low alloy steel X65 and carbon steel Q235 are widely applied as construction materials for tubings and pipelines in oil and gas industry due to their superior mechanical characteristics and cost-effectiveness. Nevertheless, the steels are very vulnerable to corrosion in environments containing CO<sub>2</sub> as well as chloride (Ali et al., 2020; Liu et al.,

2016; Hua et al., 2015; Zhao et al., 2012). Re-injection of CO<sub>2</sub> into oil and gas wells can improve the oil recovery, but the application of this technology increases the dissolution of gaseous CO<sub>2</sub> in co-produced water, resulting in the formation of CO<sub>2</sub>-saturated saline solution (Zucchi et al., 1993). The pipeline steels will suffer various forms of corrosion in this environment, leading to a tremendous waste of resources and energy. The use of inhibitors has been considered as the most economical and flexible option to reduce corrosion problems (Liu et al., 2023; Wang et al., 2022a). The employment of imidazoline and its derivatives as corrosion inhibitors has gained increasing interest owing to the advantages of low toxicity, excellent inhibition effectiveness and practical use (He et al., 2014; Wan et al., 2020; Wang et al., 2022b, 2023; Zhang et al., 2015b). It is generally accepted that the protection of metals using imidazoline-based inhibitors is mainly caused by the adsorption of their molecules on the metal surfaces to form a

\* Corresponding author.

E-mail address: [wb7411@163.com](mailto:wb7411@163.com) (B. Wang).

Peer review under responsibility of King Saud University.



Production and hosting by Elsevier

protective layer (Biswas et al., 2015; Liu et al., 2009). The effectiveness of inhibition is related to many factors including inhibitor molecular structure, composition of the aggressive environment, inhibitor concentration, as well as the surface condition and microstructure of metals (Lopez et al., 2003a; Lopez et al., 2003b).

Different microstructures (ferrite, martensite, perlite, bainite) may be formed in steels due to the differences in the fabrication process and chemical composition, and which could influence not only the corrosion resistance of steels but also the inhibitive performance of inhibitors. Some researchers have investigated the effect of steel microstructure on inhibition performance. Okafor et al. (Okafor et al., 2011) observed that a rosin amide imidazoline exhibited different inhibition performances for P110 and N80 steels due to the various structural modifications and grain sizes of steels. Oblonsky et al. (Oblonsky et al., 1995) noted that the adsorption of octadecyldimethylbenzylammonium chloride (ODBAC) was much stronger on the steel with ferritic-perlitic microstructure than that on the steel with martensitic microstructure. This result was mainly due to the formation of a more stable passivation film on the surface of martensitic steel, and which prevented the optimal adsorption of inhibitor molecules. Lopez et al. (Lopez et al., 2005) studied the performances of three imidazoline-based inhibitors for annealed steel as well as quenched and tempered (Q&T) steel. These three kinds of inhibitors displayed very different inhibition performances for the two steels, and which was mainly ascribed to the various morphology and distribution of Fe<sub>3</sub>C in the steels. Zhang et al. (Zhang et al., 2018) found that, compared with H steel (coarse laminar pearlite), the imadazoline-based inhibitor adsorbed more uniformly on T steel with shot rod and globular shaped pearlite because of the homogeneous distribution of Fe<sub>3</sub>C in the specimen, and correspondingly the inhibitor film formed on the T steel surface was more protective. The importance of the effect of steel microstructure on inhibition performance has been recognized and some research has been done for this subject, however, there is no definitive consensus on this issue. Therefore, it is necessary to carry out further research for getting a better understanding of the inhibition mechanism concerning both the inhibitor structure and the steel microstructure, and which is also very important for field applications.

In this work, the 2-phenyl imidazoline (2-PI) was applied as an eco-friendly inhibitor for Q235 and X65 steels with different microstructures. The inhibition performance of 2-PI inhibitor and its mechanism were studied through weight loss method, electrochemical tests as well as surface characterization. Additionally, the adsorption thermodynamics of the inhibitor was explored and the WBE technique was also conducted to analyze the nonuniform corrosion kinetics of both steels with and without the 2-PI inhibitor.

## 2. Experimental

### 2.1. Material preparation

In this work, the substrates used for research are Q235 and X65 steels and Table 1 lists their chemical compositions. The steel samples were mechanically cut into 10 mm × 10 mm × 3 mm and 50 mm × 10 mm × 3 mm dimensions for surface studies and weight loss tests, respectively. The working electrode of electrochemical experiments was prepared by embedding samples into epoxy resin with a retention

area of 1.0 cm<sup>2</sup>. As shown in Fig. 1, the WBE was composed by one hundred identical steel wires that were sealed with epoxy resin with an interval of 1.0 mm to insulate from each other. Before each test, the surface of WBE was abraded with SiC emery paper from 400 to 1000 grade, then cleaned with deionized water, degreased with ethanol and finally dried in a desiccator for use.

The corrosive medium was 3 wt% NaCl solution saturated with CO<sub>2</sub>, which was prepared by dissolving analytical grade NaCl in deionized water and filling with CO<sub>2</sub> gas to reach saturation. The pH of the test solution was 4.11. The 2-PI inhibitor was purchased from Adamas Reagent Co., Ltd. (Shanghai, China) and its molecular structure was exhibited in Fig. 2.

### 2.2. Weight-loss measurements

After immersion in CO<sub>2</sub>-saturated medium with and without 2-PI addition at 293–323 K for 72 h, the steel coupons were taken out and removed rust in the descaling liquid. Then, the mass losses of three parallel coupons were recorded and the corrosion rate ( $v$ , g m<sup>-2</sup>h<sup>-1</sup>) was determined:

$$v = \frac{w_1 - w_2 - w_0}{At} \quad (1)$$

where  $w_1$  and  $w_2$  are the average weights (g) before and after corrosion, respectively. Besides,  $w_0$  represents the weight loss in the course of descaling,  $A$  stands for the area of specimen surface (m<sup>2</sup>) and  $t$  indicates the immersion time (h).

### 2.3. Electrochemical experiments

The electrochemical investigations were performed on the CHI660E electrochemical system with a three-electrode cell. The working electrodes were the Q235 and X65 steels, respectively. A saturated calomel electrode (SCE) and a platinum electrode were applied as the reference and the counter, separately. Prior to the experiment, the working electrode was kept in the test solution at open circuit potential (OCP) for 1 h to reach a relative steady state. Then, the electrochemical impedance spectroscopy (EIS) was recorded at OCP in a frequency domain from 100 kHz to 0.01 Hz with a sinusoidal AC voltage of 5 mV. The polarization curves were scanned over a potential range from -250 to +250 mV versus the OCP with setting scan rate of 0.5 mV s<sup>-1</sup>.

### 2.4. WBE test

The WBE test was carried out through a multichannel zero resistance ammeter (CST520, CorrTest). The reference electrode was made of a saturated calomel electrode while the working electrode was in the form of WBE. All wires were connected to each other prior to measurement. Corrosion process was investigated by mapping galvanic currents between a chosen wire and all the other wires. Then the tendency of general

**Table 1** The chemical compositions of the studied steels (wt.%).

Steels	C	Mn	Si	P	S	Cr	Mo	Nb	Al	Cu	Co	V	Ce	Fe
Q235	0.19	0.59	0.30	0.04	0.05	–	–	–	–	–	–	–	–	Bal.
X65	0.06	1.61	0.18	0.01	–	0.13	0.05	0.05	0.03	0.03	0.05	0.04	0.38	Bal.

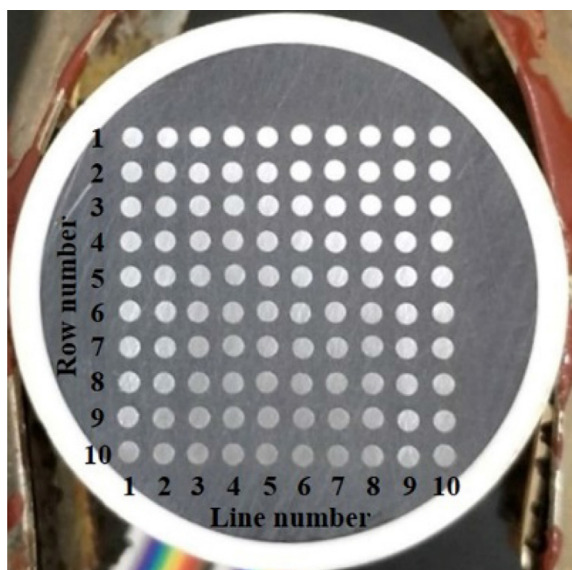


Fig. 1 Image of the WBE surface.

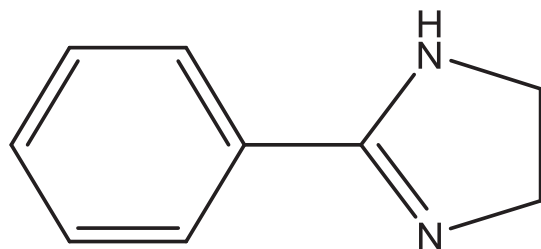


Fig. 2 The molecular structure of 2-phenyl imidazoline.

and/or localized corrosion of both steels in the test medium can be evaluated by the galvanic current data.

### 2.5. Surface analysis

Corrosion morphologies of both steels with and without 2-PI inhibitor were surveyed by FE-SEM SU-8010 microscope (Hitachi, Japan) at an acceleration voltage of 5 kV. The elementals on the steel surfaces were determined by the XPS technology through a PHI 5300 spectrometer (PerkinElmer, USA) equipped with an Al K $\alpha$  X-ray excitation source. Binding energy scale was corrected for charge effects with reference to the C 1 s peak at 284.6 eV and peak fitting was done using the XPS Peak software.

## 3. Results and discussion

### 3.1. Microstructure examination

Microstructure characterization of the two steels was analyzed by Nikon Optiphot metallographic microscope. The microstructures presented in Fig. 3 are both composed of quasi-polygonal ferrite (QF) and granular pearlite (GP) structures. The distribution of ferrite grains of both steels is not uniform. Besides, it is observed that the pearlite is distributed on

the grain boundaries of ferrite. Compared with X65 steel, the content of pearlite in Q235 steel is larger and the distribution of pearlite is more uniform.

### 3.2. Weight loss measurement

The corrosion rates of Q235 and X65 steels at different temperatures with various concentrations of 2-PI inhibitor were listed in Table 2. Among which, the inhibition efficiency ( $\eta$ ) is determined using Eq. (2):

$$\eta = \frac{v_0 - v}{v_0} \times 100\% \quad (2)$$

where  $v_0$  and  $v$  indicate the sample corrosion rates without and with the addition of 2-PI inhibitor, separately.

It is found in Table 2 that, in the absence of 2-PI, the corrosion rates of both steels are very high and increase with elevated temperature. This result is attributed to the fact that the increasing temperature can promote all the corrosion-related reactions, such as transfer of active components to steel surface, chemical and electrochemical reactions. In addition, as shown in Table 2, the corrosion rates of X65 steel are always larger than those of Q235 steel at the same temperature, and which could be ascribed to the differences in elemental compositions and microstructures between the two kinds of steels.

The corrosion rates of both steels decrease significantly after adding 2-PI inhibitor at studied temperatures, suggesting that the 2-PI inhibitor can effectively protect Q235 and X65 steels from CO<sub>2</sub> corrosion. It is evident from Fig. 4 that, at the same temperature, the  $\eta$  values enhance with increasing inhibitor concentration. The increase in concentration improves the number of the adsorbed 2-PI molecules on sample surfaces, leading to a larger coverage of the exposure area. However, as temperatures increase from 293 K to 323 K, the  $\eta$  values for both steels at the same concentration are significantly reduced. The similar phenomenon has been observed by other researchers (Berdimurodov et al., 2021; Singh et al., 2017). They have found that the elevated temperature accelerates the desorption process of inhibitor molecules from steel surfaces, resulting in a decrease in surface coverage. It is also found that, when the concentration of 2-PI is lower than 200 mg L<sup>-1</sup>, the  $\eta$  values for Q235 steel are larger than those for X65 steel at the same temperature, however, as the inhibitor concentrations exceed 200 mg L<sup>-1</sup>, the opposite trend is shown. This could be related to the change in the adsorption type of 2-PI inhibitor on the surfaces of the two steels, and which will be discussed in detail in the following sections.

### 3.3. Electrochemical measurements

#### 3.3.1. Potentiodynamic polarization experiment

The polarization curves of Q235 and X65 steels in the presence of various concentrations of 2-PI inhibitor after immersion of 24 h are displayed in Fig. 5. The relevant parameters are shown in Table 3, including anodic ( $\beta_a$ ) and cathodic ( $\beta_c$ ) Tafel slopes, corrosion current density ( $i_{\text{corr}}$ ) as well as corrosion potential ( $E_{\text{corr}}$ ). Eq. (3) is applied for determining the inhibition efficiency (Heydari and Javidi, 2012):

$$\eta = \frac{i_{\text{corr}}^0 - i_{\text{corr}}}{i_{\text{corr}}^0} \times 100\% \quad (3)$$

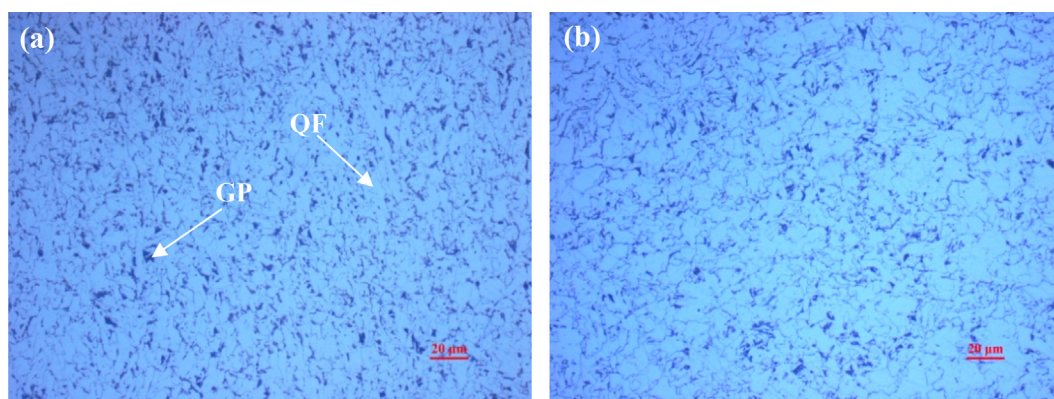


Fig. 3 Microstructures of Q235 steel (a) and X65 steel (b).

**Table 2** Corrosion parameters gained from weight loss method for both steels with different concentrations of 2-PI inhibitor at the studied temperatures.

Concentration (mg L <sup>-1</sup> )	T (K)	Q235		X65	
		$v$ (g m <sup>-2</sup> h <sup>-1</sup> )	$\eta$ (%)	$v$ (g m <sup>-2</sup> h <sup>-1</sup> )	$\eta$ (%)
0	293	0.3843	–	0.4473	–
	303	0.5166	–	0.5844	–
	313	0.6351	–	0.7090	–
	323	0.7287	–	0.7928	–
100	293	0.0980	74.5	0.1505	66.4
	303	0.1367	73.5	0.2564	56.1
	313	0.1768	72.2	0.3366	52.5
	323	0.1645	71.4	0.2467	50.9
200	293	0.0407	89.4	0.0700	85.4
	303	0.0865	83.3	0.0877	85.0
	313	0.1094	82.8	0.0898	83.3
	323	0.1280	80.4	0.2031	74.4
400	293	0.0306	92.0	0.0212	95.3
	303	0.0489	90.5	0.0458	92.2
	313	0.0785	87.7	0.0708	91.0
	323	0.1424	81.5	0.0768	90.3
700	293	0.0254	93.4	0.0140	96.9
	303	0.0509	92.2	0.0276	95.3
	313	0.0521	91.8	0.0573	92.9
	323	0.0530	90.7	0.0432	92.6
1000	293	0.0217	94.4	0.0073	98.4
	303	0.0738	93.7	0.0306	95.8
	313	0.0360	92.3	0.0309	94.6
	323	0.0441	92.0	0.0398	94.0

where  $i_{\text{corr}}$  and  $i_{\text{corr}}^0$  represent the corrosion current densities in the presence and absence of 2-PI inhibitor, separately.

It is obvious from Fig. 5 that both the anodic and cathodic current densities of the two steels decrease observably after the addition of 2-PI inhibitor, indicating that not only the anodic dissolution of the steels but also the cathodic reaction are retarded. According to Table 3, the  $E_{\text{corr}}$  values shift to positive direction with increasing 2-PI concentration, and the maximum positive displacements of  $E_{\text{corr}}$  values of both steels are smaller than 85 mV. It is indicated according to the previous research works (Shahmoradi et al., 2021; Verma et al., 2021; Tao et al., 2012) that the 2-PI inhibitor functions as a mixed-type inhibitor and inhibits the anodic process more effectively. Also, as seen in Table 3, the change trends of inhi-

bitation efficiencies of 2-PI inhibitor for both steels are uniform with the weight loss results.

### 3.3.2. EIS tests

The aftereffect of corrosion inhibitors is very important for the practical application, but few studies have been carried out regarding this kind of issue in previous works (Zhu et al., 2022; Dewangan et al., 2022). Thus EIS method was conducted in this work for characterizing the growth and decay law of 2-PI inhibitor film on Q235 and X65 steels within the immersion time of 168 h, and the plots are depicted in Fig. 6. The Nyquist plots for both steels without 2-PI addition and the plot of Q235 steel with the immersion time of 144 h exhibit a depressed semicircle in high frequency region and a tail with

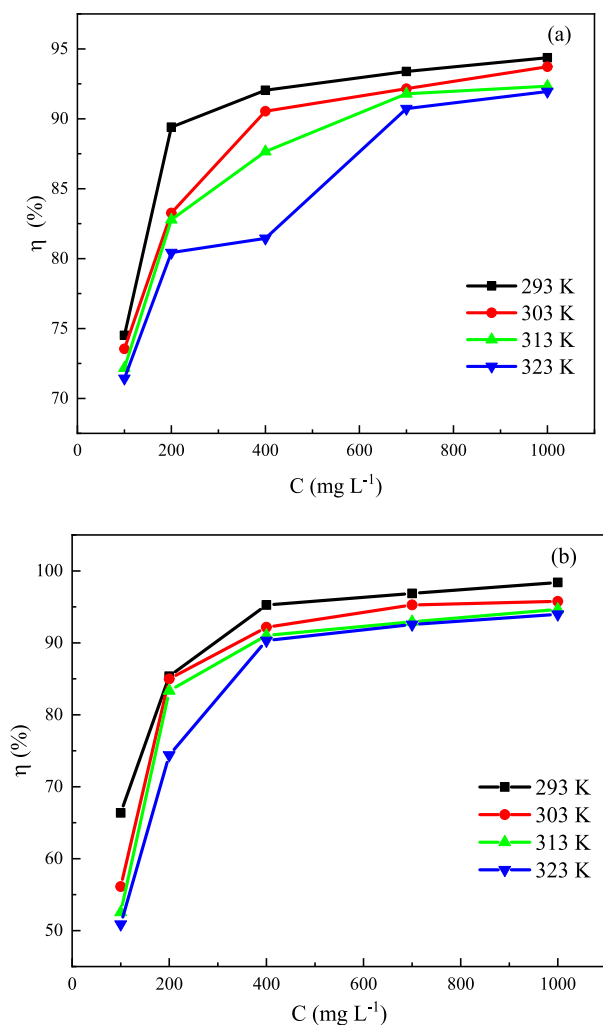


**Fig. 4** The variation of inhibition efficiency ( $\eta$ ) with inhibitor concentration ( $C$ ) at different temperatures for Q235 steel (a) and X65 steel (b).

an angle of about 45° to the real-axis in low frequency region. The tail is caused by the diffusion process of working electrode and is the characteristic of the so-called Warburg impedance.

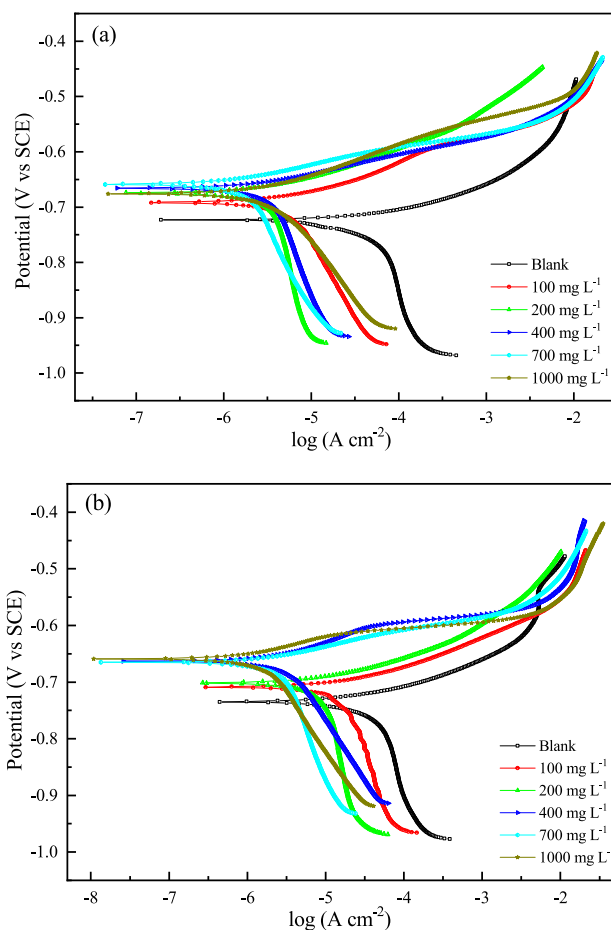


**Fig. 5** Polarization curves of Q235 (a) and X65 (b) steels in the test solutions with different concentrations of 2-PI at 293 K.

The plots of X65 steel in the presence of 2-PI with the soaking times of 120, 144 and 168 h and the plot of Q235 steel with the immersion time of 120 h present an inductive loop at low frequencies and a depressed semicircle in middle-to-high frequencies. The presentation of an inductive loop is thought to be due to the adsorption of FeOH<sub>ads</sub> in the corrosion process (Wang et al., 2019; Calderon et al., 2017). All the other Nyquist plots

**Table 3** Electrochemical parameters for Q235 and X65 steels with the addition of various concentrations of 2-PI at 293 K.

Steels	C (mg L <sup>-1</sup> )	$E_{\text{corr}}$ (mV vs.SCE)	$\beta_a$ (mV dec <sup>-1</sup> )	$\beta_c$ (mV dec <sup>-1</sup> )	$i_{\text{corr}}$ ( $\mu\text{A cm}^2$ )	$\eta$ (%)
Q235	0	-724	39.1	-230.7	35.75	-
	100	-692	68.8	-275.5	7.16	75.1
	200	-675	56.0	-312.6	2.98	91.7
	400	-676	57.6	-112.9	2.46	93.1
	700	-666	35.9	-178.8	2.09	94.2
	1000	-659	36.2	-157.9	1.13	96.8
X65	0	-735	59.0	-265.6	45.83	-
	100	-709	57.5	-416.9	23.56	48.6
	200	-702	46.1	-287.7	8.95	80.5
	400	-664	50.5	-212.3	2.71	94.1
	700	-665	32.6	-163.1	1.54	96.6
	1000	-659	35.4	-52.6	0.69	98.5

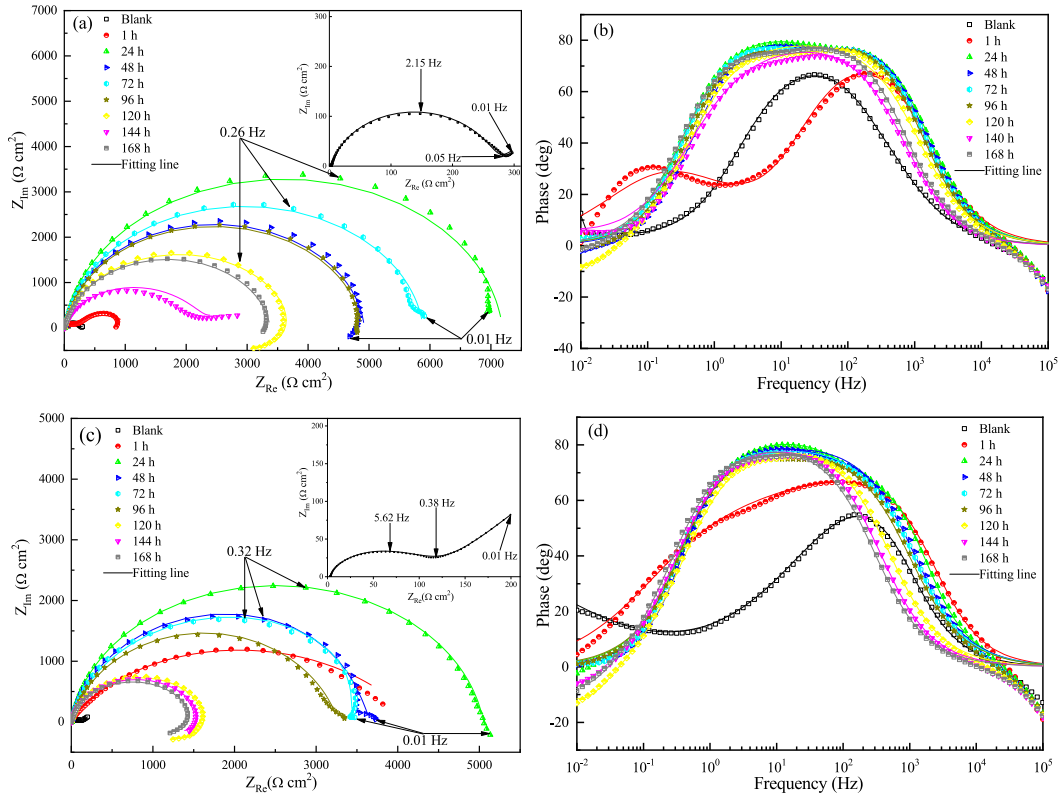


**Fig. 6** Nyquist and Bode plots for both steels in the test solutions with 1000 mg L<sup>-1</sup> 2-PI in different test periods: (a, b) Q235 steel and (c, d) X65 steel.

in Fig. 6 appear as a depressed semicircular shape with the center below the real axis, and this is due to the frequency dispersion effect induced by the inhomogeneities and roughness of working electrode surface (Nam et al., 2013; Wang et al., 2018).

As exhibited in Fig. 6 (b) and (d), after addition of 2-PI inhibitor, the Bode plot of Q235 steel after 1 h immersion show two peaks and all the other plots display a wide peak, which demonstrates that there are two time constants. Thus the EIS data can be simulated using the equivalent circuits in Fig. 7. In which,  $R_s$  stands for solution resistance,  $R_f$  is protective film resistance,  $R_1 + R_2$  represent the charge transfer resis-

tance  $R_{ct}$ ,  $Z_w$  is Warburg impedance,  $L$  is inductance. CPE stands for the constant phase element that is employed for fitting more accurately. CPE<sub>1</sub> and CPE<sub>2</sub> represent the double layer capacitance and the film capacitance, separately. The corresponding parameters are summarized in Table 4, in which the double layer capacitance ( $C_{dl}$ ) and inhibition efficiency ( $\eta$ ) can be determined using the equations given below (Wang et al., 2020):

$$C_{dl} = Y_0 (2\pi f_{max})^{n-1} \quad (4)$$

$$\eta = \frac{R_{ct} - R_{ct}^0}{R_{ct}} \times 100\% \quad (5)$$

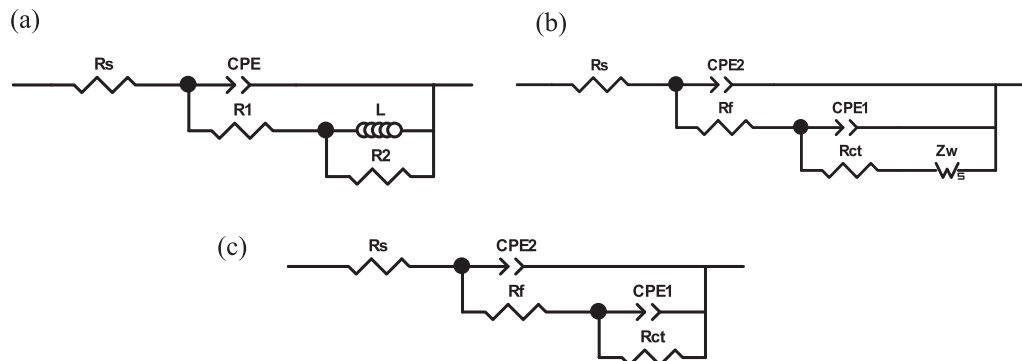


**Fig. 7** Equivalent circuit models for fitting of EIS data.

**Table 4** Impedance fitting values for Q235 and X65 steels in the test solutions containing 1000 mg L<sup>-1</sup> 2-PI in different test periods at 293 K.

Samples	Time	$C_{dl}$ ( $n_1$ )	$R_{ct}$	$R_f$	$\eta$
	(h)	( $\mu\text{F cm}^{-2}$ )	( $\Omega \text{ cm}^2$ )	( $\Omega \text{ cm}^2$ )	(%)
Uninhibited Q235	1	645.9 (0.64)	276.0	30.6	–
Inhibited Q235	1	231.2 (0.66)	918.4	181.9	70.0
	24	18.0 (0.91)	6867.0	518.5	96.0
	48	21.4 (0.94)	4593.0	327.0	94.0
	72	25.4(0.92)	5502.0	501.9	95.0
	96	26.0 (0.95)	4378.0	382.4	93.7
	120	109.3 (0.90)	3798.0	–	92.7
	144	106.5 (0.69)	2150.0	135.7	87.2
	168	45.1 (0.93)	2724.0	351.5	90.0
Uninhibited X65	1	1137.0 (0.49)	124.9	12.8	–
Inhibited X65	1	286.1 (0.62)	4213.0	319.0	97.0
	24	51.9 (0.86)	5014.0	533.5	97.5
	48	42.5 (0.89)	3614.0	370.6	96.5
	72	40.9 (0.89)	3678.0	393.2	96.6
	96	43.1 (0.88)	3054.0	294.5	95.9
	120	243.4 (0.91)	1692.2	–	92.6
	144	321.3 (0.91)	1604.2	–	92.2
	168	384.5 (0.91)	1515.3	–	91.8

where  $Y_0$  and  $n$  represent the CPE constant as well as CPE exponent, separately.  $f_{\max}$  is ascribed to the frequency at which there has the maximum value of imaginary impedance.  $R_{ct}$  and  $R_{ct}^0$  are the charge transfer resistances of the inhibited and uninhibited samples, respectively.

The  $R_{ct}$  and  $R_f$  values of the inhibited samples increase sharply within 24 h, indicating that the steel corrosion is retarded effectively by the adsorption of 2-PI molecules, and the maximum inhibition efficiencies for Q235 and X65 steels are 96.0% and 97.5%, separately. In addition, it is noticed that the inhibition efficiency for X65 steel after 1 h immersion is as high as 97.0%, suggesting that the adsorption rate of 2-PI molecules on X65 steel surface is very rapid, and which is much faster than the adsorption of 2-PI molecules on Q235 steel surface. In contrast, a diminution of the  $C_{dl}$  values is observed after the addition of 2-PI inhibitor for both steels, and this can be ascribed to the fact that the 2-PI molecules replace the water molecules at the steel/solution interface and then form an adsorption film (Zhao et al., 2020).

After 24 h immersion, the  $R_{ct}$  values decrease slightly with extension of soaking time except for a few fluctuating values, which suggests that the adsorbed 2-PI molecules are desorbed or rearranged on sample surfaces until achieving the dynamic equilibrium of adsorption and desorption. However, even after 168 h of test, the  $\eta$  values for Q235 and X65 steels are still up to 90.0% and 91.8%, separately, proving that the 2-PI inhibitor has long-lasting protective effect for Q235 and X65 steels.

### 3.4. Adsorption isotherm

The interfacial information between adsorbed inhibitor and steel surface can be elucidated by different adsorption isotherms. In this present study, the adsorption mechanism of 2-PI is legitimately described by Langmuir adsorption model:

$$\frac{C}{\theta} = \frac{1}{K_{ads}} + C \quad (6)$$

where  $C$  corresponds to inhibitor concentration,  $\theta$  stands for surface coverage determined from weight-loss data and  $K_{ads}$  represents adsorption equilibrium constant. Fig. 8 displays the plots for  $C/\theta - C$  and the relevant parameters are summed up in Table 5. The results show that the obtained regression coefficients ( $R^2$ ) and the slop values are both close to unity at the studied temperatures, indicating that the adsorption of 2-PI molecules on Q235 and X65 steels follows Langmuir adsorption isotherm. The  $K_{ads}$  values can be determined based on the intercept of the straight lines. The  $K_{ads}$  values decrease noticeably with temperature, showing that the increased temperature promotes the desorption process of 2-PI molecules from sample surfaces (Yang et al., 2019; Solomon et al., 2019), and this result coincides well with the measured result of weight loss test that the inhibition efficiencies of 2-PI inhibitor decrease with temperature.

Based on the  $K_{ads}$  values, the standard free energy of adsorption ( $\Delta G_{ads}^0$ ) is calculated as follow:

$$K_{ads} = \frac{1}{55.5} \exp\left(\frac{-\Delta G_{ads}^0}{RT}\right) \quad (7)$$

where 55.5 denotes the molar concentration of water solvent expressed in mol L<sup>-1</sup>,  $R$  stands for molar gas constant, and  $T$  corresponds to temperature in K. The standard adsorption enthalpy ( $\Delta H_{ads}^0$ ) can be obtained according to the Van't Hoff equation:

$$\frac{d \ln K_{ads}}{dT} = \frac{\Delta H_{ads}^0}{RT^2} \quad (8)$$

And the indefinite integral is expressed as:

$$\ln K_{ads} = -\frac{\Delta H_{ads}^0}{RT} + \text{constant} \quad (9)$$

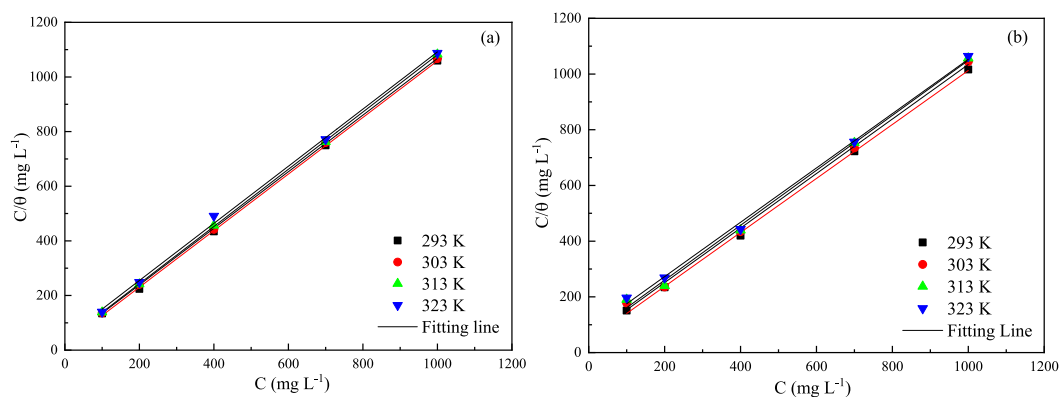


**Fig. 8** Langmuir adsorption plots for Q235 (a) and X65 (b) steels in  $\text{CO}_2$  saturated solutions containing various concentrations of 2-PI at the studied temperatures.

**Table 5** Thermodynamic parameters of 2-PI adsorption on Q235 and X65 steels at the studied temperatures.

Steels	$T$ (K)	$R^2$	Slope	$K_{\text{ads}}$ ( $\text{L mol}^{-1}$ )	$\Delta G_{\text{ads}}^0$ ( $\text{kJ mol}^{-1}$ )	$\Delta H_{\text{ads}}^0$ ( $\text{kJ mol}^{-1}$ )	$\Delta S_{\text{ads}}^0$ ( $\text{J mol}^{-1} \text{K}^{-1}$ )
Q235	293	0.9998	1.04	6286.17	-31.09	-16.38	50.20
	303	0.9999	1.04	4619.60	-31.37		49.49
	313	0.9999	1.05	4356.46	-32.26		50.73
	323	0.9979	1.05	3201.56	-32.40		49.79
X65	293	0.9993	0.97	3362.37	-29.57	-14.58	51.13
	303	0.9970	0.98	2631.42	-29.66		49.75
	313	0.9960	0.99	2339.04	-30.64		51.29
	323	0.9969	0.98	1885.85	-31.04		50.94

The  $\ln K_{\text{ads}}$  is plotted against  $1000 T^{-1}$  as shown in Fig. 9. The  $\Delta H_{\text{ads}}^0$  can be obtained from the slope. Then the Gibbs-Helmholtz equation can be used for determining the standard adsorption entropy ( $\Delta S_{\text{ads}}^0$ ):

$$\Delta G_{\text{ads}}^0 = \Delta H_{\text{ads}}^0 - T\Delta S_{\text{ads}}^0 \quad (10)$$

The calculated thermodynamic parameters are also exhibited in Table 5. The negative  $\Delta G_{\text{ads}}^0$  values indicate that the adsorption process of 2-PI molecules over the Q235 and X65 steels surfaces occurs spontaneously under the experimental

temperatures (Li et al., 2019). In the present study, the  $\Delta G_{\text{ads}}^0$  values are calculated from  $-32.59$  to  $-29.69$   $\text{kJ mol}^{-1}$ , suggesting that the adsorption of 2-PI molecules on both steels is a mixture of physisorption and chemisorption (Qian and Cheng, 2019; Wang et al., 2021). Besides, the negative values of  $\Delta H_{\text{ads}}^0$  shows that the adsorption of 2-PI molecules is an exothermic process accompanied by release of energy, and which also proves that elevated temperature is not conducive to the adsorption of 2-PI inhibitor. The calculated values of  $\Delta S_{\text{ads}}^0$  are all positive without obvious changes at the studied

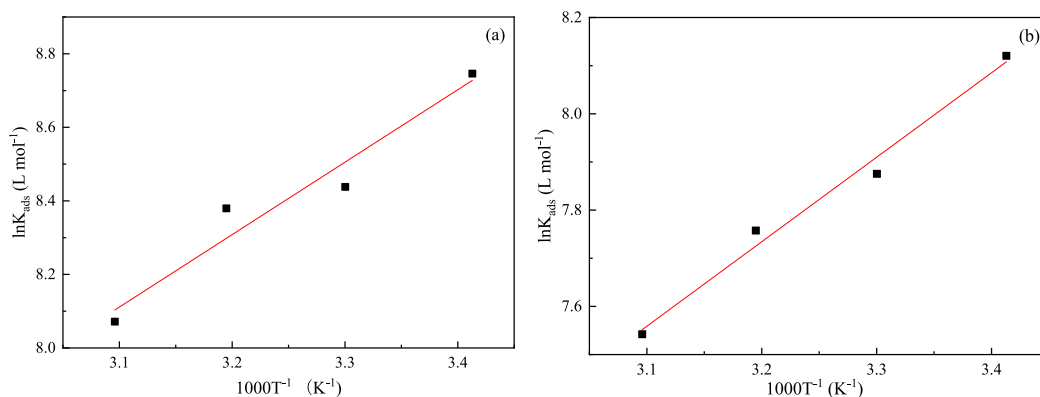


**Fig. 9** Plots of  $\ln K$  versus  $1/T$  for Q235 (a) and X65 (b) steels in the test solutions.

temperatures, indicating that the adsorption process of 2-PI is accompanied with an entropy increase, and which has been thought to be the driving force for the adsorption of inhibitor molecules on metal surfaces (Zhang et al., 2012).

Based on the above calculated thermodynamic parameters, the adsorption mechanism of 2-PI inhibitor on Q235 and X65 steels can be deduced. In acid solution, the two N atoms in the imidazoline ring of 2-PI molecule can be protonated as shown in Fig. 10 (He et al., 2014; Shamsa et al., 2022). The protonated 2-PI inhibitor can physically adsorb onto the negatively charged steel surface or on the positively charged surface via anions (CO<sub>3</sub><sup>2-</sup>, HCO<sub>3</sub><sup>-</sup>, Cl<sup>-</sup>) (Wang et al., 2011b). In the later case, the anions are considered as the connecting bridge between the protonated 2-PI molecules and the positively charged surface (Xu et al., 2014; Zhang et al., 2015a). In addition to the physisorption form, there should also be chemisorption process for the inhibitor covering the steel surface. As shown in Fig. 11, the 2-PI molecules can adsorb on Q235 and X65 steels by sharing long-pair electrons in 1-N and 3-N atoms and/or  $\pi$  electrons in the imidazoline ring with the vacant 3d-orbitals of Fe atom to form coordinate covalent bonds. Meanwhile, the  $\pi^*$ -orbitals of 2-PI inhibitor can also accept d-electrons of Fe atom to form feedback bonds (Wang et al., 2011a). Besides, the benzene ring containing  $\pi$  bond in the 2-PI molecule can also combine with Fe atom due to its strong electron donor moiety. Thus, the 2-PI inhibitor can form polycentric chemical sorption on the sample surfaces, and which will be further proved by the results of XPS analysis.

Furthermore, taking the results of weight loss method and electrochemical experiments into consideration, it can be inferred that the adsorption ability of 2-PI inhibitor on Q235 steel surface is better than that of X65 steel surface at lower concentrations. However, the opposite trend is observed at higher concentrations. When the inhibitor concentration is less than 200 mg L<sup>-1</sup>, there is sufficient H<sup>+</sup> in the test solution to

make the 2-PI molecules undergo protonation reaction. Therefore, most 2-PI molecules exist in the protonation forms at low concentrations, and the adsorption process in this case is mainly physical adsorption. However, with further increase in inhibitor concentration, there are more and more 2-PI molecules in the test solution, while the H<sup>+</sup> concentration in the test solution is relatively stable. Therefore, more and more 2-PI molecules will not undergo protonation reaction, and the adsorption process in this situation is mainly chemical adsorption. Meanwhile, combined with the result of microstructural observation (Fig. 3), it can be inferred that the higher pearlite/ferrite ratio of Q235 steel promotes the physical adsorption of the protonated 2-PI molecules at lower concentrations and the lower pearlite/ferrite ratio of X65 steel enhances the chemical adsorption of the unprotonated 2-PI molecules at higher concentrations. Thus, the 2-PI inhibitor has better inhibition effect on Q235 steel at lower concentrations and on X65 steel at higher concentrations.

### 3.5. Surface analysis

#### 3.5.1. XPS characterization

The XPS spectra for Q235 and X65 samples after 24 h immersion in CO<sub>2</sub> saturated solutions with and without 1000 mg L<sup>-1</sup> 2-PI are recorded in Fig. 12. The wide-scale XPS spectrum from Fig. 12(a) shows that the inhibited samples contain O, Fe, C and N elements on the surfaces, among which the existence of N and C peaks supplies evidence of the adsorption of 2-PI molecules on sample surfaces. The high-resolution spectra for C 1 s are fitted with three peaks as given in Fig. 12(b) and (d). Taking Fig. 12(b) as an example, the lower binding energy at 284.57 eV is assigned to C–C and C–H structures, and the peak at 285.48 eV is corresponding to C–N structure. Besides, the peak at 289.03 eV is associated with the C = N and C = O bonds, among which the C = O bond results mainly from the corrosion products such as FeCO<sub>3</sub>.

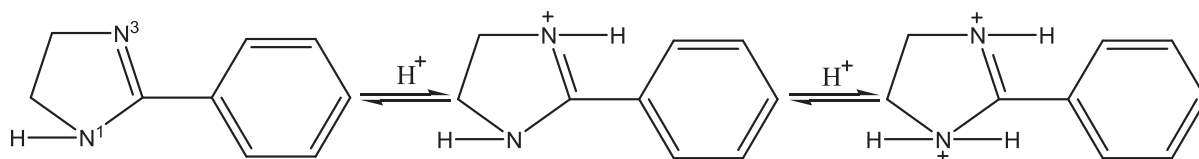


Fig. 10 Graphical representation for protonation of 2-PI molecules in acidic solution.

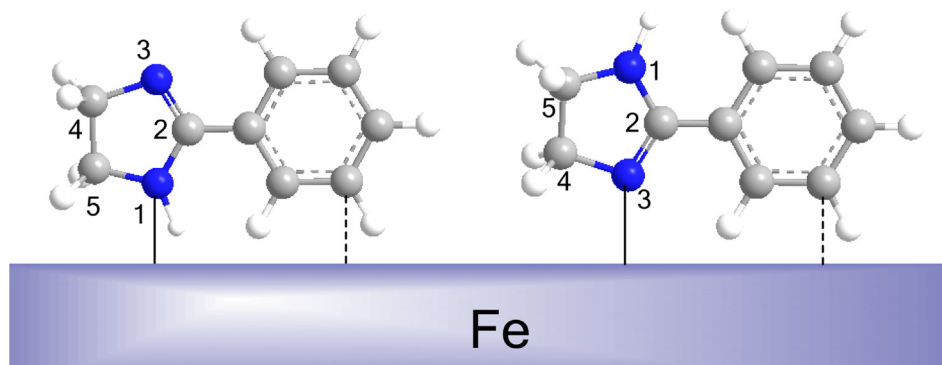
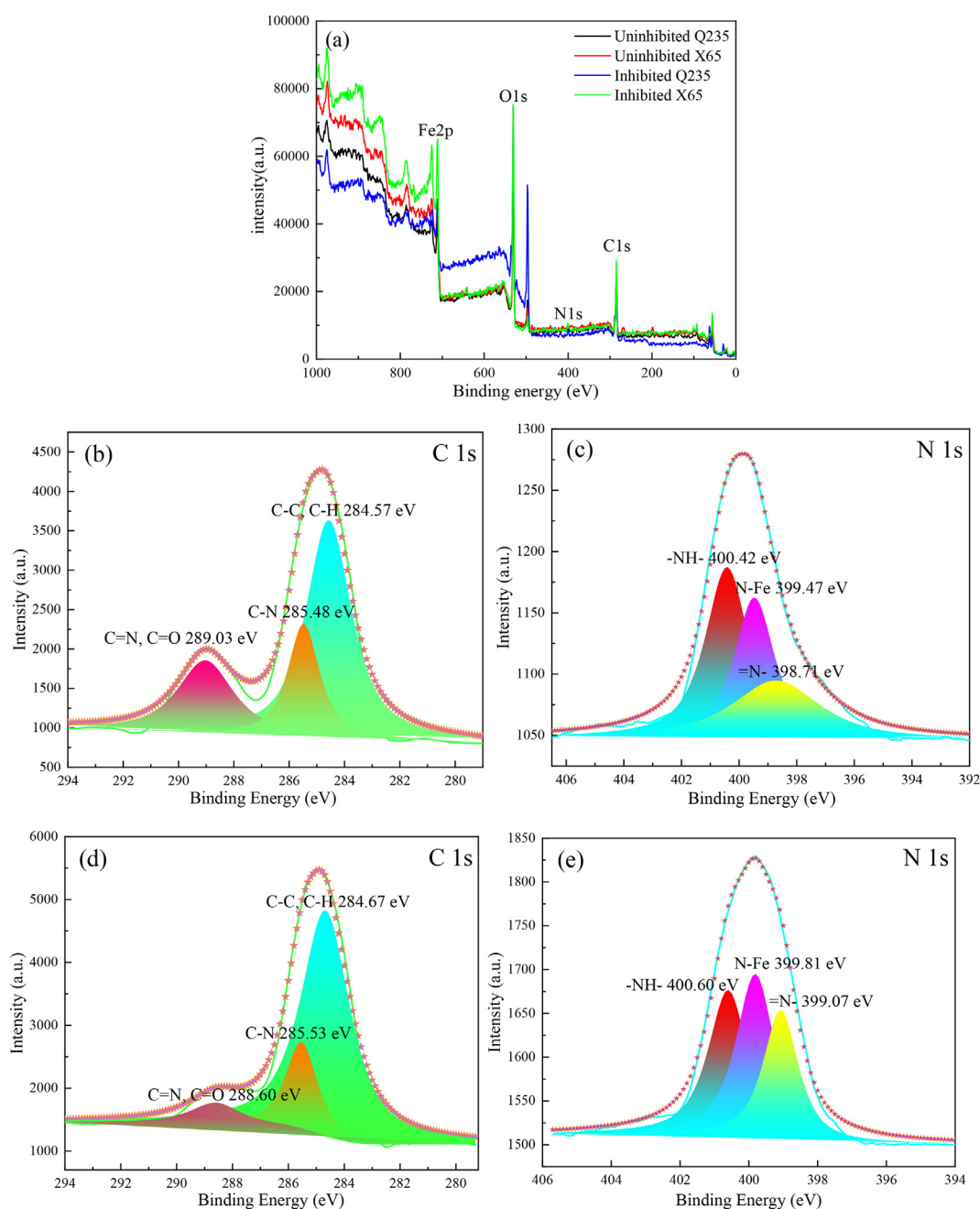


Fig. 11 Schematic presentation of the chemical adsorption of 2-PI molecules on steel surface.



**Fig. 12** (a) XPS spectrum for uninhibited and inhibited Q235 and X65 steels at 293 K; C 1s (b) and N 1s (c) for 2-PI treated Q235 steel; C1s (d) and N 1s (e) for 2-PI treated X65 steel.

The heteroatom N in the imidazoline ring with lone-pair electrons can accept electrons from iron and can also provide electrons to 3d-orbitals of iron to form covalent bonds (Wang et al., 2011a). From Fig. 12(c) and (e), the N 1s high-resolution spectra of Q235 and X65 steels are fitted with three signal peaks, separately. The signal peaks lying at 399.47 eV and 399.81 eV are attributed to the N-Fe structures, which confirm the chemisorption of 2-PI molecules on the steel surfaces (Bentiss et al., 2009; Tourabi et al., 2013). In addition, taking Fig. 12(c) as an example, the other two signal peaks located at 400.42 eV and 398.71 eV are ascribed to the struc-

tures of -NH- as well as =N- in the imidazoline ring of 2-PI molecule, respectively. Furthermore, it is noteworthy that the observed intensity of N 1s peak of 2-PI treated X65 steel is higher than that of 2-PI treated Q235 steel, which confirms again that the 2-PI inhibitor has stronger chemisorption ability on X65 steel surface at higher concentrations.

### 3.5.2. SEM observation

Fig. 13 shows the SEM micrographs of Q235 and X65 steels after 24 h immersion in CO<sub>2</sub> saturated solutions with and without 1000 mg L<sup>-1</sup> 2-PI at 293 K and 323 K. It is noticed that the

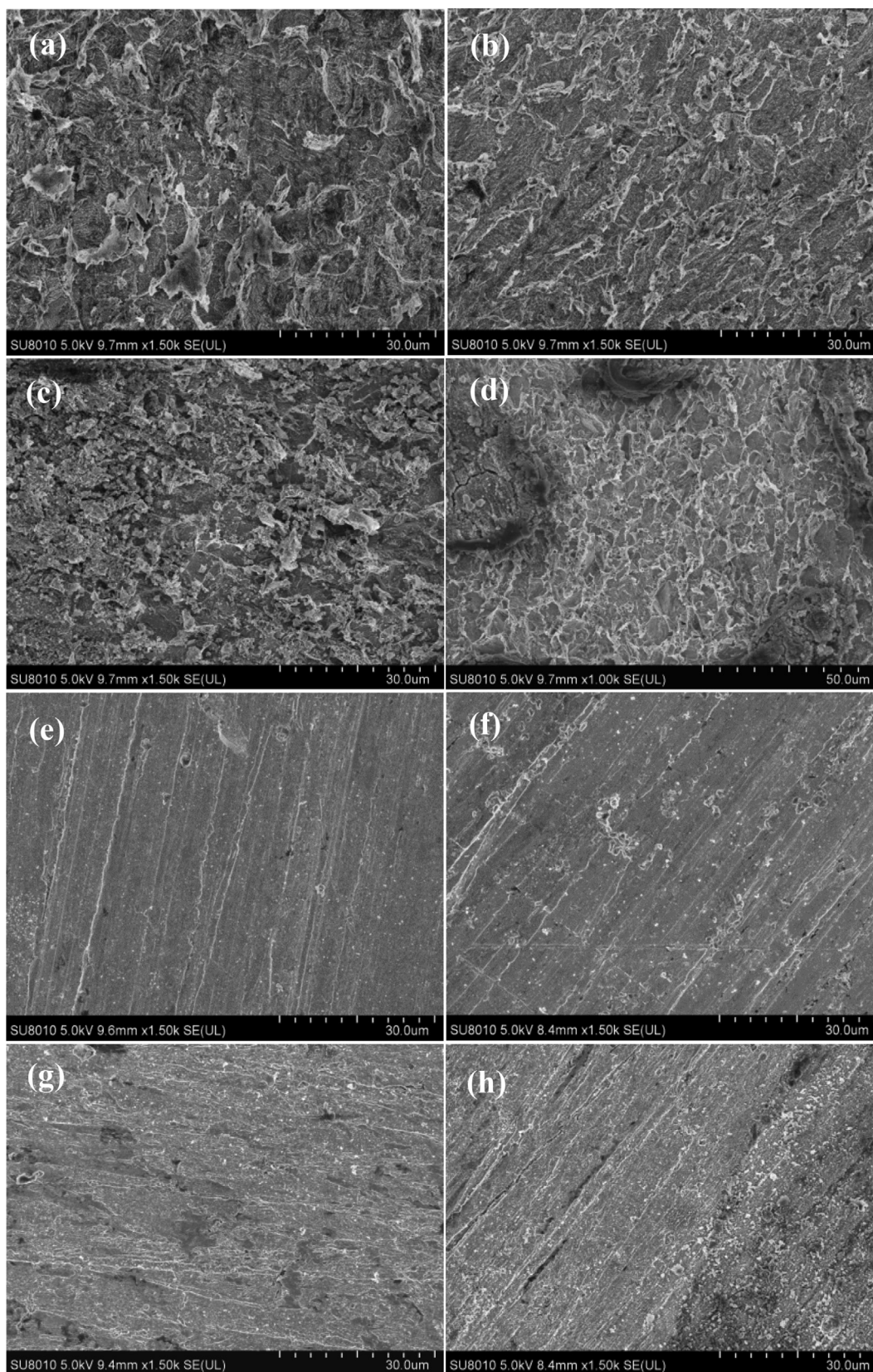


**Fig. 13** SEM images of the samples after 24 h immersion in CO<sub>2</sub> saturated solutions without and with 1000 mg L<sup>-1</sup> 2-PI: uninhibited Q235 steel at 293 K (a) and 323 K (c); uninhibited X65 steel at 293 K (b) and 323 K (d); inhibited Q235 steel at 293 K (e) and 323 K (g); inhibited X65 steel at 293 K (f) and 323 K (h).

uninhibited samples of both steels show very damaged and roughened surfaces, and the surface morphologies of which are significantly different. The Q235 steel is mainly subject to general corrosion with no sign of localized corrosion, and the corrosion products of which are with lamellar structures at 293 K but with granular structures at 323 K. As to X65 steel, in addition to general corrosion, this steel also suffers typical localized corrosion at 323 K, just as shown in Fig. 13 (d). In contrast, the surfaces of all the inhibited steels are smooth and even the original grinding scratches are visible at the studied temperatures, indicating the excellent corrosion inhibition ability of 2-PI inhibitor for the two steels against general and localized corrosion.

### 3.6. WBE test

The kinetics of nonuniform corrosion of Q235 and X65 steels in CO<sub>2</sub>-saturated solutions was studied by the WBE method. The corrosion process of WBE was determined by measuring the galvanic current, as displayed in Fig. 14, and the relevant parameters are listed in Table 6. In which, the localized corrosion dissolution of the most active anode can be characterized by the value of maximum anodic current density and the total anodic current density is related to the general corrosion degree of WBE (Manh et al., 2019; Nam et al., 2018). As exhibited in Fig. 14, the maps show the characteristics of large numbers of minor anodes and cathodes and the positions of

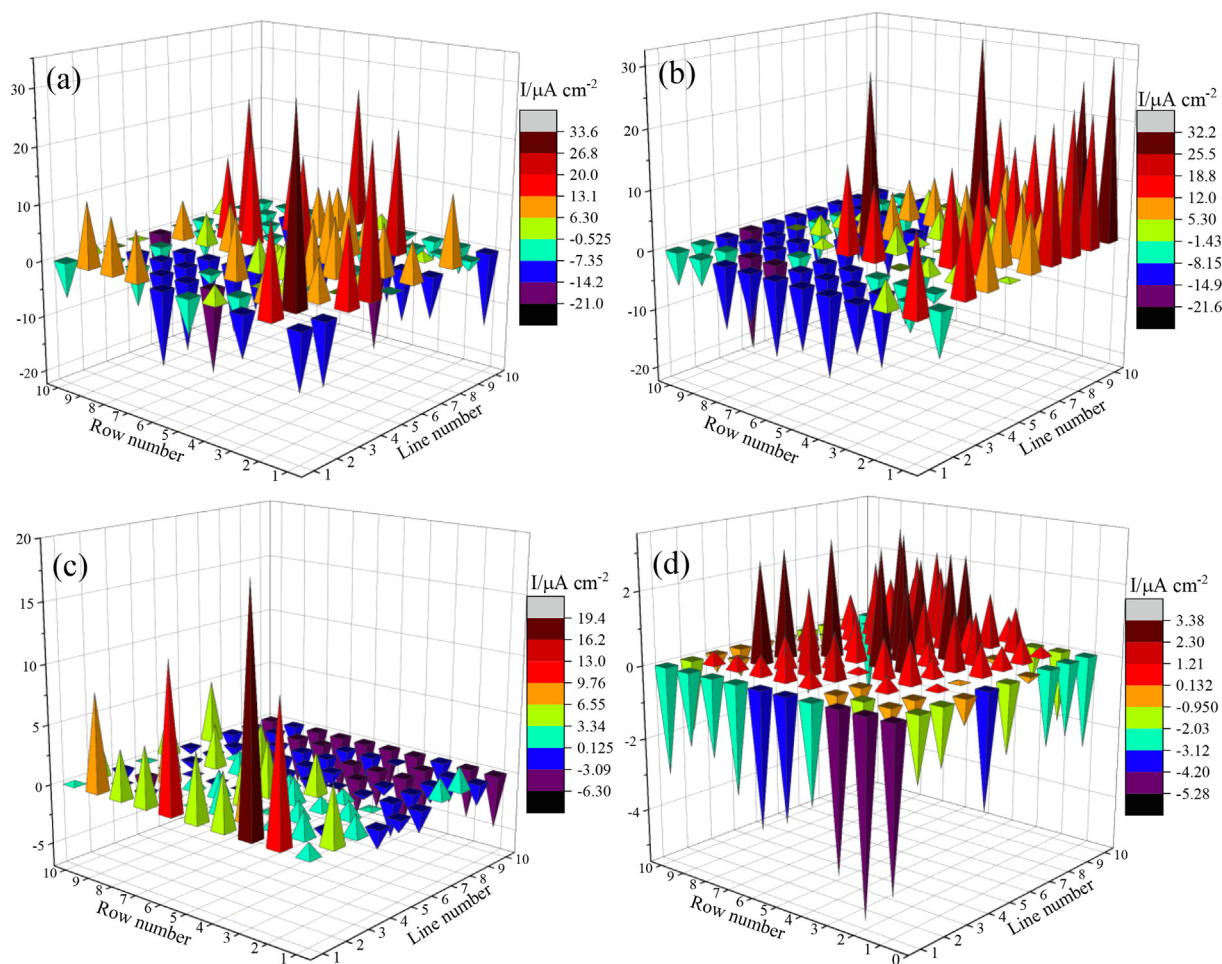


**Fig. 14** Galvanic current distribution maps recorded on the WBE surfaces of both steels in the test solutions: Q235 (a) and X65 (b) steels without inhibitor; Q235 (c) and X65 (d) steels with 1000 mg L<sup>-1</sup> inhibitor.

**Table 6** Related values gained from the WBE test.

Samples	Maximum anodic current density ( $\mu\text{A cm}^{-2}$ )	Maximum cathodic current density ( $\mu\text{A cm}^{-2}$ )	Total anodic current density ( $\mu\text{A cm}^{-2}$ )
Uninhibited Q235	33.41	-20.81	445.74
Inhibited Q235	19.44	-6.21	158.52
Uninhibited X65	32.01	-21.57	505.25
Inhibited X65	3.38	-5.28	77.04

which are changed randomly. After adding the 2-PI inhibitor to the solutions, the current densities of almost all electrodes decrease obviously, indicating the inhibition effect of both the anode and cathode reactions, and which is also in keeping with the characteristics of mixed type inhibitor of 2-PI. From Table 6, the maximum anodic dissolution current densities of uninhibited and inhibited Q235 and X65 steels decrease from 33.41 and 32.01  $\mu\text{A cm}^{-2}$  to 19.44 and 3.38  $\mu\text{A cm}^{-2}$ , respectively, suggesting that the 2-PI inhibitor has superior inhibition effect on the localized corrosion of both steels, and which is very consistent with the results of SEM test. Furthermore, the total anodic current densities are also noticeably reduced after addition of 2-PI inhibitor, which confirms again the inhibition effect of 2-PI on the general corrosion of both steels.

#### 4. Conclusions

This study comparatively analyzed the inhibition performances of the 2-PI inhibitor for Q235 and X65 steels with various microstructures in CO<sub>2</sub>-saturated solution. The findings of this study are summarized as follows:

- (1) The 2-PI compound is demonstrated to be a mixed-type inhibitor that suppresses the anodic reaction more effectively. Additionally, it manifests durable and superior inhibition effects for Q235 and X65 steels against general and localized corrosion.
- (2) The 2-PI inhibitor displays better inhibition performance for Q235 steel at lower concentrations and for X65 steel at higher concentrations. The inhibition efficiencies of 2-PI increase with the augment of concentration but decrease with the elevated temperature.
- (3) The adsorption of 2-PI inhibitor on both steels is in accordance with the Langmuir rule and involves both physisorption and chemisorption. The thermodynamic data signify the spontaneous and exothermic nature of the adsorption process, accompanied with an entropy increase.
- (4) The Q235 steel with a higher pearlite/ferrite ratio promotes the physical adsorption of the protonated 2-PI molecules at lower concentrations, whereas the X65 steel with a lower pearlite/ferrite ratio enhances the chemical adsorption of the unprotonated 2-PI molecules at higher concentrations.

#### Declaration of Competing Interest

The authors declare that they have no known competing financial interests or personal relationships that could have appeared to influence the work reported in this paper.

#### Acknowledgements

This work is supported by the National Natural Science Foundation of China (Nos. 51901096 and 51971192) and by the Equipment Pre-research Field Fund (80904020507).

#### References

Ali, S.A., Mazumder, M.A.J., Nazal, M.K., Al-Muallem, H.A., 2020. Assembly of succinic acid and isoxazolidine motifs in a single entity to mitigate CO<sub>2</sub> corrosion of mild steel in saline media. *Arab. J. Chem.* 13, 242–257.

Bentiss, F., Jama, C., Mernari, B., Attari, H.E., Kadi, L.E., Lebrini, M., Traisnel, M., Lagrenée, M., 2009. Corrosion control of mild

steel using 3,5-bis(4-methoxyphenyl)-4-amino-1,2,4-triazole in normal hydrochloric acid medium. *Corros. Sci.* 51, 1628–1635.

Berdimurodov, E., Kholikov, A., Akbarov, K., Guo, L., Abdullah, A. M., Elik, M., 2021. A gossypol derivative as an efficient corrosion inhibitor for St2 steel in 1 M HCl + 1 M KCl: An experimental and theoretical investigation. *J. Mol. Liq.* 328, 115475.

Biswas, A., Pal, S., Udayabhanu, G., 2015. Experimental and theoretical studies of xanthan gum and its graft co-polymer as corrosion inhibitor for mild steel in 15% HCl. *Appl. Surf. Sci.* 353, 173–183.

Calderon, J.A., Vasquez, F.A., Carreno, J.A., 2017. Adsorption and performance of the 2-mercaptobenzimidazole as a carbon steel corrosion inhibitor in EDTA solutions. *Mater. Chem. Phys.* 185, 218–226.

Dewangan, Y., Verma, D.K., Berdimurodov, E., Haldhar, R., Dagdag, O., Tripathi, M., Mishra, V.K., Kumar, P.A., 2022. N-hydroxypyrazine-2-carboxamide as a new and green corrosion inhibitor for mild steel in acidic medium: experimental, surface morphological and theoretical approach. *J. Adhes. Sci. Technol.* 36, 2644–2664.

He, X.K., Jiang, Y.M., Li, C., Wang, W.C., Hou, B.L., Wu, L.Y., 2014. Inhibition properties and adsorption behavior of imidazole and 2-phenyl-2-imidazoline on AA5052 in 1.0 M HCl solution. *Corros. Sci.* 83, 124–136.

Heydari, M., Javidi, M., 2012. Corrosion inhibition and adsorption behaviour of an amido-imidazoline derivative on API 5L X52 steel in CO<sub>2</sub>-saturated solution and synergistic effect of iodide ions. *Corros. Sci.* 61, 148–155.

Hua, Y., Barker, R., Neville, A., 2015. Comparison of corrosion behavior for X-65 carbon steel in supercritical CO<sub>2</sub>-saturated water and water-saturated/unsaturated supercritical CO<sub>2</sub>. *J. Supercrit. Fluid.* 97, 224–237.

Li, Y., Zhang, S.W., Ding, Q., Qin, B.F., Hu, L.T., 2019. Versatile 4,6-dimethyl-2-mercaptopyrimidine based ionic liquids as high-performance corrosion inhibitors and lubricants. *J. Mol. Liq.* 284, 577–585.

Liu, X.H., Gao, Y.H., Gao, Y.G., Yang, Y., Li, W.T., Ma, N., Zhao, J.Q., 2023. Synthesis of polyaspartic acid-glycidyl adduct and evaluation of its scale inhibition performance and corrosion inhibition capacity for Q235 steel applications. *Arab. J. Chem.* 16, 104515.

Liu, H.W., Gu, T.Y., Zhang, G.A., Wang, W., Dong, S., Chen, Y.F., Liu, H.F., 2016. Corrosion inhibition of carbon steel in CO<sub>2</sub>-containing oilfield produced water in the presence of iron-oxidizing bacteria and inhibitors. *Corros. Sci.* 105, 149–160.

Liu, X., Okafor, P.C., Zheng, Y.G., 2009. The inhibition of CO<sub>2</sub> corrosion of N80 mild steel in single liquid phase and liquid/particle two-phase flow by aminoethyl imidazoline derivatives. *Corros. Sci.* 51, 744–751.

Lopez, D.A., Schreiner, W.H., de Sanchez, S.R., Simison, S.N., 2003a. The influence of carbon steel microstructure on corrosion layers-An XPS and SEM characterization. *Appl. Surf. Sci.* 207, 69–85.

Lopez, D.A., Simison, S.N., de Sanchez, S.R., 2003b. The influence of steel microstructure on CO<sub>2</sub> corrosion EIS studies on the inhibition efficiency of benzimidazole. *Electrochim. Acta* 48, 845–854.

Lopez, D.A., Simison, S.N., de Sanchez, S.R., 2005. Inhibitors performance in CO<sub>2</sub> corrosion EIS studies on the interaction between their molecular structure and steel microstructure. *Corros. Sci.* 47, 735–755.

Manh, T.D., Hien, P.V., Nguyen, Q.B., Quyen, T.N., Hinton, B.R.W., Nam, N.D., 2019. Corrosion inhibition of steel in naturally-aerated chloride solution by rare-earth 4-hydroxycinnamate compound. *J. Taiwan Inst. Chem. Eng.* 103, 177–189.

Nam, N.D., Bui, Q.V., Mathesh, M., Tan, M.Y.J., Forsyth, M., 2013. A study of 4-carboxyphenylboronic acid as a corrosion inhibitor for steel in carbon dioxide containing environments. *Corros. Sci.* 76, 257–266.

- Nam, N.D., Hien, P.V., Hoai, N.T., Thu, V.T.H., 2018. A study on the mixed corrosion inhibitor with a dominant cathodic inhibitor for mild steel in aqueous chloride solution. *J. Taiwan Inst. Chem. Eng.* 91, 556–569.
- Oblonsky, L.J., Chesnut, G.R., Devine, T.M., 1995. Adsorption of octadecyldimethylbenzylammonium chloride to two carbon steel microstructures as observed with surface-enhanced raman spectroscopy. *Corrosion* 51, 891–900.
- Okafor, P.C., Liu, C.B., Zhu, Y.J., Zheng, Y.G., 2011. Corrosion and corrosion inhibition behavior of N80 and P110 carbon steel in CO<sub>2</sub>-saturated simulated formation water by rosin amide imidazoline. *Ind. Eng. Chem. Res.* 50, 7273–7281.
- Qian, S., Cheng, Y.F., 2019. Synergism of imidazoline and sodium dodecylbenzenesulphonate inhibitors on corrosion inhibition of X52 carbon steel in CO<sub>2</sub>-saturated chloride solutions. *J. Mol. Liq.* 294, 111674.
- Shahmoradi, A.R., Ranjbarhane, M., Javidparvar, A.A., Guo, L., Berdimurodov, E., Ramezanzadeh, B., 2021. Theoretical and surface/electrochemical investigations of walnut fruit green husk extract as effective inhibitor for mild-steel corrosion in 1M HCl electrolyte. *J. Mol. Liq.* 338, 116550.
- Shamsa, A., Barmatov, E., Hughes, T.L., Hua, Y., Neville, A., Barker, R., 2022. Hydrolysis of imidazoline based corrosion inhibitor and effects on inhibition performance of X65 steel in CO<sub>2</sub> saturated brine. *J. Petrol. Sci. Eng.* 208, 109235.
- Singh, A., Ansari, K.R., Kumar, A., Liu, W.Y., Chen, S.S., Lin, Y.H., 2017. Electrochemical, surface and quantum chemical studies of novel imidazole derivatives as corrosion inhibitors for J55 steel in sweet corrosive environment. *J. Alloys. Compd.* 712, 121–133.
- Solomon, M.M., Umoren, S.A., Quraishi, M.A., Salman, M., 2019. Myristic acid based imidazoline derivative as effective corrosion inhibitor for steel in 15% HCl medium. *J. Colloid. Interf. Sci.* 551, 47–60.
- Tao, Z., He, W., Wang, S., Zhang, S., Zhou, G., 2012. A study of differential polarization curves and thermodynamic properties for mild steel in acidic solution with nitrophenyltriazole derivative. *Corros. Sci.* 60, 205–213.
- Tourabi, M., Nohair, K., Traisnel, M., Jama, C., Bentiss, F., 2013. Electrochemical and XPS studies of the corrosion inhibition of carbon steel in hydrochloric acid pickling solutions by 3,5-bis(2-thienylmethyl)-4-amino-1,2,4-triazole. *Corros. Sci.* 75, 123–133.
- Verma, D.K., Kazi, M., Alqahtani, M.S., Syed, R., Berdimurodov, E., Kaya, S., Salim, R., Asatkar, A., Haldhar, R., 2021. N-hydroxybenzothioamide derivatives as green and efficient corrosion inhibitors for mild steel: Experimental, DFT and MC simulation approach. *J. Mol. Struct.* 1241, 130648.
- Wan, S., Ma, X.Z., Miao, C.H., Zhang, X.X., Dong, Z.H., 2020. Inhibition of 2-phenyl imidazoline on chloride-induced initial atmospheric corrosion of copper by quartz crystal microbalance and electrochemical impedance. *Corros. Sci.* 170, 108692.
- Wang, B., Du, M., Zhang, J., Gao, C.J., 2011a. Electrochemical and surface analysis studies on corrosion inhibition of Q235 steel by imidazoline derivative against CO<sub>2</sub> corrosion. *Corros. Sci.* 53, 353–361.
- Wang, B., Du, M., Zhang, J., Li, C.J., Liu, J., Liu, H.X., Li, R.R., Li, Z.R., 2019. Corrosion inhibition of mild steel by the hydrolysate of an imidazoline-based inhibitor in CO<sub>2</sub>-saturated solution. *Rsc. Adv.* 9, 36546–36557.
- Wang, G., Li, W.T., Wang, X., Yuan, X.W., Yang, H.Y., 2023. A Mannich-base imidazoline quaternary ammonium salt for corrosion inhibition of mild steel in HCl solution. *Mater. Chem. Phys.* 293, 126956.
- Wang, S., Sun, J., Shan, B.R., Fan, W.J., Ding, R., Yang, J., Zhao, X.D., 2022a. Performance of dodecyl dimethyl benzyl ammonium chloride as bactericide and corrosion inhibitor for 7B04 aluminum alloy in an aircraft fuel system. *Arab. J. Chem.* 15, 103926.
- Wang, L., Wang, B., Luo, L.Z., Jiang, H., Liu, J., 2020. Atmospheric corrosion behavior of 7A09 aluminum alloy exposed to an industrial environment. *Mater. Corros.* 71, 1971–1979.
- Wang, X.Z., Wang, B., Wang, Q.Y., Li, R.R., Liu, H.X., Jiang, H., Liu, J., 2021. Inhibition effect and adsorption behavior of two pyrimidine derivatives as corrosion inhibitors for Q235 steel in CO<sub>2</sub>-saturated chloride solution. *J. Electroanal. Chem.* 903, 115827.
- Wang, X.T., Yang, J., Chen, X., Liu, C., Zhao, J.W., 2022b. Synergistic inhibition properties and microstructures of self-assembled imidazoline and phosphate ester mixture for carbon steel corrosion in the CO<sub>2</sub> brine solution. *J. Mol. Liq.* 357, 119140.
- Wang, X.M., Yang, H.Y., Wang, F.H., 2011b. An investigation of benzimidazole derivative as corrosion inhibitor for mild steel in different concentration HCl solutions. *Corros. Sci.* 53, 113–121.
- Wang, B., Zhang, L.W., Jiang, H., Li, X.B., Mu, X.L., 2018. Atmospheric corrosion comparison of antirust aluminum exposed to industrial and coastal atmospheres. *Mater. Corros.* 69, 1516–1525.
- Xu, B., Yang, W.Z., Liu, Y., Yin, X.S., Gong, W.N., Chen, Y.Z., 2014. Experimental and theoretical evaluation of two pyridinecarboxaldehyde thiosemicarbazone compounds as corrosion inhibitors for mild steel in hydrochloric acid solution. *Corros. Sci.* 78, 260–268.
- Yang, D.P., Ye, Y.W., Su, Y., Liu, S., Gong, D.R., Zhao, H.C., 2019. Functionalization of citric acid-based carbon dots by imidazole toward novel green corrosion inhibitor for carbon steel. *J. Clean. Prod.* 229, 180–192.
- Zhang, H.H., Pang, X.L., Gao, K.W., 2018. Localized CO<sub>2</sub> corrosion of carbon steel with different microstructures in brine solutions with an imidazoline-based inhibitor. *Appl. Surf. Sci.* 442, 446–460.
- Zhang, H.H., Pang, X.L., Zhou, M., Liu, C., Wei, L., Gao, K.W., 2015a. The behavior of pre-corrosion effect on the performance of imidazoline-based inhibitor in 3 wt.% NaCl solution saturated with CO<sub>2</sub>. *Appl. Surf. Sci.* 356, 63–72.
- Zhang, J., Song, W.W., Shi, D.L., Niu, L.W., Li, C.J., Du, M., 2012. A dissymmetric bis-quaternary ammonium salt gemini surfactant as effective inhibitor for Q235 steel in hydrochloric acid. *Prog. Org. Coat.* 75, 284–291.
- Zhang, K.G., Xu, B., Yang, W.Z., Yin, X.S., Liu, Y., Chen, Y.Z., 2015b. Halogen-substituted imidazoline derivatives as corrosion inhibitors for mild steel in hydrochloric acid solution. *Corros. Sci.* 90, 284–295.
- Zhao, J.M., Chen, G.H., 2012. The synergistic inhibition effect of oleic-based imidazoline and sodium benzoate on mild steel corrosion in a CO<sub>2</sub>-saturated brine solution. *Electrochim. Acta* 69, 247–255.
- Zhao, T.Y., Munis, A., Zheng, M.S., Hu, J., Teng, H.P., Wei, L.P., 2020. 2-(2-Pentadecyl-4, 5-dihydro-1H-imidazol-1-yl)ethanol as a sustainable inhibitor for copper corrosion in molten hydrated phase change materials. *J. Mol. Liq.* 316, 113927.
- Zhu, M., Guo, L., He, Z., Marzouki, R., Zhang, R.H., Berdimurodov, E., 2022. Insights into the newly synthesized N-doped carbon dots for Q235 steel corrosion retardation in acidizing media: A detailed multidimensional study. *J. Colloid. Interf. Sci.* 608, 2039–2049.
- Zucchi, F., Trabanelli, G., Brunoro, G., Monticelli, C., Rocchini, G., 1993. Corrosion inhibition of carbon and low alloy steels in sulphuric acid solutions by 2-mercaptopyrimidine derivatives. *Mater. Corros.* 44, 264–268.